ARTICLES
https://doi.org/10.1038/s41929-021-00589-y

nature catalysis

Check for updates

Mechanistic investigation of Rh(I)-catalysed asymmetric Suzuki–Miyaura coupling with racemic allyl halides

Lucy van Dijk[1,8], Ruchuta Ardkhean[1,2,8], Mireia Sidera[1,3,8], Sedef Karabiyikoglu[1], Özlem Sari[1,4,5], Timothy D. W. Claridge[1]✉, Guy C. Lloyd-Jones[6]✉, Robert S. Paton[1,7]✉ and Stephen P. Fletcher[1]✉

Understanding how catalytic asymmetric reactions with racemic starting materials can operate would enable new enantioselective cross-coupling reactions that give chiral products. Here we propose a catalytic cycle for the highly enantioselective Rh(I)-catalysed Suzuki–Miyaura coupling of boronic acids and racemic allyl halides. Natural abundance ^{13}C kinetic isotope effects provide quantitative information about the transition-state structures of two key elementary steps in the catalytic cycle, transmetallation and oxidative addition. Experiments with configurationally stable, deuterium-labelled substrates revealed that oxidative addition can happen via *syn*- or *anti*-pathways, which control diastereoselectivity. Density functional theory calculations attribute the extremely high enantioselectivity to reductive elimination from a common Rh complex formed from both allyl halide enantiomers. Our conclusions are supported by analysis of the reaction kinetics. These insights into the sequence of bond-forming steps and their transition-state structures will contribute to our understanding of asymmetric Rh–allyl chemistry and enable the discovery and application of asymmetric reactions with racemic substrates.

Suzuki–Miyaura cross-coupling is used extensively for C(sp^2)–C(sp^2) bond formation (Fig. 1a). One reason for the broad adaptation of this method is the wide range of organoboron reagents that are readily available and easy to handle, provides advantages over other organometallic reagents[1]. Since the first report in 1979, tremendous effort has been directed towards further development, which led to Suzuki's receipt of the 2010 Nobel Prize in Chemistry alongside Heck and Negishi[2].

The development of asymmetric cross-coupling transformations with organoboron reagents is an area of active investigation. Reported strategies include starting from single enantiomer alkylboronates, enantiopure electrophiles and desymmetrizations[3]. Boronic acids and derivatives have been employed in enantioselective allylic arylations, mostly catalysed by Rh (refs [4,5]), Cu (ref. [6]), Pd (ref. [7]) and Ni (ref. [8]). Some stereospecific allylic arylations have also been developed using Pd (ref. [9]) and Cu (ref. [10]).

We developed a highly enantioselective Suzuki-type coupling between arylboronic acids and racemic cyclic allyl halides catalysed by Rh–bisphosphine complexes (Fig. 1b)[11]. We also demonstrated the use of vinyl and (hetero)arylboronic acids in combination with racemic (hetero)cyclic electrophiles[12]. The versatility of the method was highlighted by synthesis of the natural product (+)-isoananbasine[12] and the anticancer agent niraparib (Fig. 1b)[13]. However, this transformation is currently limited to electrophiles that, after cleavage of the carbon–halogen bond, are achiral about the allyl unit[13,14].

Detailed mechanistic studies on Rh-catalysed asymmetric additions are scarce. Hayashi et al. reported a key study on the additions of arylboronic acids to cyclic α,β-unsaturated ketones[15]. For that transformation, after transmetallation, 2-cyclohexenone inserts into the Rh–aryl bond to form an oxa-π-allyl Rh species, which hydrolyses to release the product. A subsequent kinetic study revealed that transmetallation from boron to Rh was the rate-determining step[16].

Asymmetric allylic addition reactions with racemic electrophiles may occur *via* several distinct mechanistic pathways. Dynamic kinetic asymmetric transformations (DYKATs) catalysed by Pd using stabilized nucleophiles occur via a well-understood mechanism; both enantiomers of the starting material are converted into a common pseudo-prochiral intermediate, and a subsequent outer-sphere addition of the nucleophile creates the new stereogenic centre[17]. A similar DYKAT mechanism was proposed to be operative in some Rh-catalysed allylic substitution reactions in which oxidative addition of both enantiomers of the substrate is the first step in the catalytic cycle and results in a Rh–allyl species[18]. Cu-catalysed asymmetric additions of alkyl zirconium reagents to racemic allylic substrates[19], in contrast with Pd-catalysed mechanisms, involve dynamic kinetic resolution facilitated by a Cu–halide–ligand complex[20]. The complex acts to interconvert enantiomers of the allyl chloride, as well as catalyse addition, and one enantiomer reacts more readily to give an enantioenriched product. Other mechanisms of catalytic asymmetric additions with racemic starting materials include various radical processes[21,22] and direct enantioconvergent processes in which the two starting enantiomers react via different mechanistic pathways to give the same enantiomer of the product[23].

To further understand the limitations and potential of Rh-catalysed asymmetric additions and of catalytic processes that

[1]Department of Chemistry, Chemistry Research Laboratory, University of Oxford, Oxford, UK. [2]Faculty of Medicine and Public Health, HRH Princess Chulabhorn College of Medical Science, Chulabhorn Royal Academy, Bangkok, Thailand. [3]Vertex Pharmaceuticals (Europe) Ltd, Milton Park, UK. [4]Department of Chemistry, Middle East Technical University, Ankara, Turkey. [5]Department of Chemistry, Kirsehir Ahi Evran University, Kirsehir, Turkey. [6]EaStChem, University of Edinburgh, Edinburgh, UK. [7]Department of Chemistry, Colorado State University, Fort Collins, CO, USA. [8]These authors contributed equally: Lucy van Dijk, Ruchuta Ardkhean, Mireia Sidera. ✉e-mail: tim.claridge@chem.ox.ac.uk; guy.lloyd-jones@ed.ac.uk; Robert.Paton@colostate.edu; stephen.fletcher@chem.ox.ac.uk

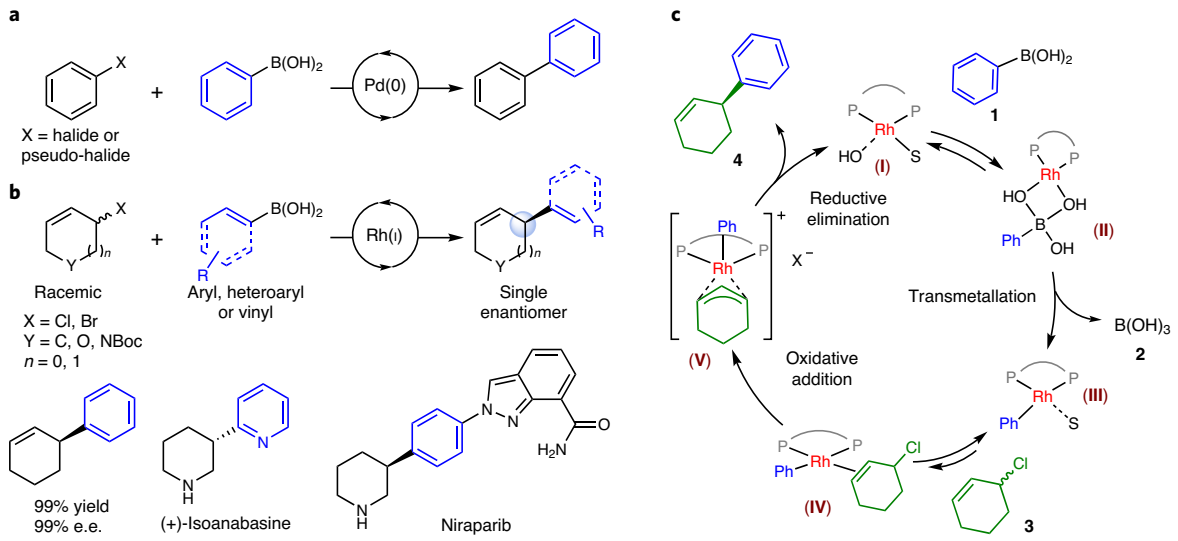

Fig. 1 | Suzuki–Miyaura cross-coupling. a, Classical Suzuki–Miyaura coupling. **b**, The enantioselective Rh-catalysed Suzuki–Miyaura coupling to form C(sp^3)–C(sp^2) bonds and selected compounds that can be synthesized using this method. **c**, A simplified catalytic cycle showing the proposed mechanism in this work with the key steps, which include transmetallation, oxidative addition and reductive elimination.

involve racemic substrates, we set out to design a series of experimental and computational experiments to reveal the mechanisms involved in this transformation. Here we discuss our experimental and computational studies that rule out the mechanistic scenarios outlined above, and instead are fully consistent with the proposal shown in Fig. 1c. The available evidence is congruent with the scenario in which a monomeric active catalytic species (**I**) reacts with the arylboronic acid (**1**) to form a Rh–aryl intermediate (**III**). Irreversible oxidative addition with both allyl chloride enantiomers yields a common η^3 complex (**V**), although one enantiomer of **3** reacts faster than the other. The subsequent reductive elimination step is enantiodetermining and sets the configuration of the product, as dictated by the absolute stereochemistry of the ligand.

Results

Preliminary NMR spectroscopic and mechanistic experiments. NMR spectroscopy was used to examine the reaction between $[Rh(cod)(OH)]_2$ (cod, cyclooctadiene) and (*S*)-Xylyl-P-Phos ((*S*)-**L1**) in THF-d_8. By comparing our data with those in literature reports[15], we identified the formation of the precatalytic species $[Rh(\mathbf{L1})(OH)]_2$ and the mixed $[Rh_2(cod)(\mathbf{L1})(OH)_2]$ dimer. The Rh–ligand dimer $[Rh(\mathbf{L1})(OH)]_2$ undergoes a rapid reaction with phenylboronic acid to give a Rh–aryl species. In contrast, when allyl chloride **3** was added to $[Rh(\mathbf{L1})(OH)]_2$, no reaction was observed, even on heating. These observations are not consistent with mechanisms initiated by the allylic electrophile first reacting with a metal complex[18].

Strikingly, the formation of the precatalyst $[Rh(\mathbf{L1})(OH)]_2$ did not give a single clean species and was often accompanied by varying amounts of other species that featured ^{31}P singlet peaks at 25.7, 24.2 and −14.7 ppm, which we attribute to mono- and dioxidized forms of the ligand. Attempts to further characterize this reaction using in situ NMR spectroscopy were hindered by the formation of complex mixtures of species that contained phosphorous, which was not overcome by using alternative Rh complexes.

In related Cu-catalysed transformations, we observed the interconversion of substrate enantiomers[20]. The Rh-catalysed arylation here could operate via a related mechanism that involves facile interconversion of substrate enantiomers followed by a stereospecific addition step. To examine whether this occurred here, we used ^{1}H NMR exchange spectroscopy. However, under the reaction conditions, no exchange between vinylic and allylic protons in **3** was observed on the NMR timescale, which suggests that the allyl chloride enantiomers do not interconvert via an S_N2' mechanism or do so at a much slower rate than the ^{1}H NMR relaxation. Therefore, a dynamic kinetic resolution mechanism appears unlikely. This does not preclude racemization occurring during these reactions—it simply suggests that this is not a fundamental requirement of the reaction. A limitation of this experiment is that interconversion via S_N2 mechanisms cannot be detected.

To better understand the active catalytic species, we probed for non-linear effects by measuring the enantiomeric excess (e.e.) of product **4** as a function of that of ligand **L1**[24]. A linear correlation between the enantiopurity of **L1** and **4** was observed, which provides no evidence for the involvement of high-order aggregates of the catalyst, consistent with an active catalytic species monomeric in Rh and **L1** (Supplementary Fig. 1).

Rh-catalysed hydroarylation and Rh-catalysed processes that involve diene electrophiles are known[25–27]. A mechanism could be operative here in which elimination of the allyl halide forms a diene intermediate, which then undergoes hydroarylation with a Rh–aryl species. To test if the reaction could occur via the formation of an intermediate diene species, we used cyclohexa-1,3-diene in place of **3** but observed no arylated product. A reaction using d_5-phenylboronic acid showed the deuterium labels remained on the phenyl ring, which rules out mechanisms that involve the insertion of the Rh catalyst into C–H bonds of the aromatic ring[26].

Transmetallation. To probe the transmetallation step, we carried out a series of competition experiments using different arylboronic acids. There is a strong positive correlation between the ratio of products obtained and the Hammett substituent constants (σ values) of the arylboronic acids (Fig. 2)[28,29]. This indicates that transmetallation is faster with electron-withdrawing substituents on the arylboronic acid, which allows electron-deficient aryl species to preferentially and irreversibly enter the catalytic cycle and leads to the formation of one product in excess. This preferential transmetallation could be due to an increased Lewis acidity of the boron, which favours formation of the boronate, and/or to an enhanced ability of electron-poor substrates to stabilize a partial negative charge during

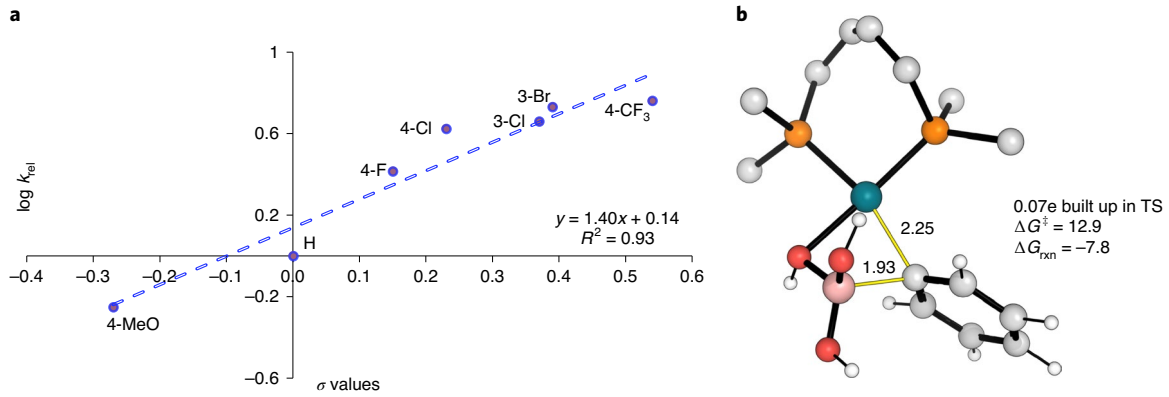

Fig. 2 | Examining the transmetallation step using experimental and computational techniques. a, A Hammett plot constructed from the results of competition experiments between various *meta*- and *para*-substituted arylboronic acids. k_{rel}, relative rate. **b**, The DFT-computed transmetallation TS (ωB97X-D/6-31G(d), LANL2DZ(f)). $\Delta G^{\ddagger}$, activation energy; ΔG_{rxn}, change in Gibbs free energy.

transmetallation[30,31]. We surmised that a key role of the base in these reactions is to aid in the formation of boronate species. Consistent with our experimental observations, the accumulation of negative charge in the aromatic ring was observed in the density functional theory (DFT)-computed transition structure (TS). Relative to the pretransmetallation intermediate with a Rh–O–B linkage[31,32], this elementary step is exergonic by 7.8 kcal mol^{-1}, consistent with irreversibility.

Natural abundance ^{13}C kinetic isotopic effects. We next focused our attention on the subsequent reaction between aryl–Rh species (**III**) and allyl chloride **3**, for which various possible mechanisms can be envisaged. To gain more understanding, we sought to determine natural abundance ^{12}C/^{13}C ratios using the method developed by Singleton and co-workers[33,34]. This approach has been employed with great success to measure competitive intermolecular ^{13}C kinetic isotope effects (KIEs) in mechanistic studies of catalytic reactions[35–43]. This commonly relies on running the reaction to high conversion and examining the ^{12}C/^{13}C ratio in the recovered starting material. However, in the asymmetric addition to **3**, the isolation of small amounts of starting material at high conversions is not possible as **3** is too sensitive to be reliably purified and may be configurationally labile during the reaction or work-up conditions[20]. It is also plausible that the two enantiomers of **3** could undergo conversion at different rates, and so confound analysis of the KIE by examining the starting material. We therefore chose to determine ^{12}C/^{13}C ratios generated in product **4** when the reaction is quenched at a low conversion and quantify the depletion of ^{13}C by quantitative ^{13}C NMR spectroscopy.

We performed the reactions on a 7.0 mmol scale as a relatively large amount of product is required for quantitative ^{13}C NMR spectroscopy and the reaction must be stopped at a low conversion to ensure the product is enriched in the faster-reacting isotope. However, using the optimized conditions at this scale at 60 °C, the reaction was much faster than anticipated; when the reaction was quenched after two minutes, the conversion was already 60%. Suitable results could be obtained by stirring the reaction at 40 °C and quenching after 20 seconds. We repeated the process three times under these conditions, with experiments giving 10, 11 and 17% conversion (Fig. 3a). For the quantitative ^{13}C spectroscopy, we took C5 as the reference carbon. Although ^{13}C KIEs are intrinsically small (ranging from 0.98 to 1.10) (ref. [44]), after running these experiments in triplicate we observed appreciable KIEs at positions C1, C3 and C7 (Fig. 3a).

For multistep catalytic mechanisms, any observed isotope effects are the result of isotopic fractionation that occurs at or before the first irreversible step that involves that reaction component[45]. Experimentally, we measured the largest KIEs at C7 (1.027 ± 0.006) and C3 (1.024 ± 0.003), and a smaller, but non-negligible, KIE was obtained at C1 (1.010 ± 0.005). As the transmetallation step is irreversible, ^{12}C fractionation at the aryl ipso-carbon (C7) of the product is most probably the result of a KIE in this elementary step.

To interpret the enrichment observed at C1 and C3, we calculated the ^{12}C/^{13}C KIE that would result from various addition mechanisms (S_N2, S_N2' and reversible *anti*-oxidative addition). The KIE values were calculated according to transition-state theory by applying the Bigeleisen–Mayer equation using scaled vibrational frequencies[46,47]. The calculated results for the most likely mechanism, as judged by comparing experimental and theoretical results, are shown in Fig. 3b–d.

In our proposed DYKAT mechanism with *anti*-oxidative addition followed by reductive elimination, there are two plausible scenarios; one in which the oxidative addition is reversible and reductive elimination is the first irreversible step that involves **3** (Fig. 3b), and another in which oxidative addition is the first irreversible step in which **3** is involved (Fig. 3c). In the first scenario (Fig. 3b), the calculated KIE of C1 is 1.013, but there is no appreciable KIE at C3. The calculated KIE of only two carbons are within the experimental errors of the measured KIEs. In the second scenario, in which the oxidative addition is irreversible, the calculated KIE starting with (*S*)-**3** gave a value of 1.035 on C3, whereas that with (*R*)-**3** gave a value of 1.029 on C1 (Fig. 3c). If both enantiomers of **3** undergo an irreversible oxidative addition, albeit at different rates, the observed KIE from the product analysis will be a weighted average from both starting enantiomers. From our calculations, a 3.3:1 ratio of (*S*)- to (*R*)-**3** undergoing oxidative addition accounts quantitatively for the experimentally observed KIE on all six carbons of the allyl unit (Fig. 3d).

These experiments are inconsistent with other possible mechanisms for the Rh-catalysed process. Overall, the ^{13}C KIEs support a mechanism in which the first step in the catalytic cycle is an irreversible transmetallation, followed by an irreversible *anti*-oxidative addition in which the enantiomers of **3** react at different rates.

DFT calculations. DFT calculations[48] were performed using the ωB97X-D functional[49]. In geometry optimizations, the LANL2DZ(f) (orbital exponent of 1.35) effective core potential (ECP)/valence double-ζ basis set was used for Rh and the split-valence 6–31G(d) basis set was used for other atoms. Single-point energy corrections were obtained with an implicit description of the reaction medium by the SMD solvent model at the ωB97X-D/6-311+G(d,p) level of

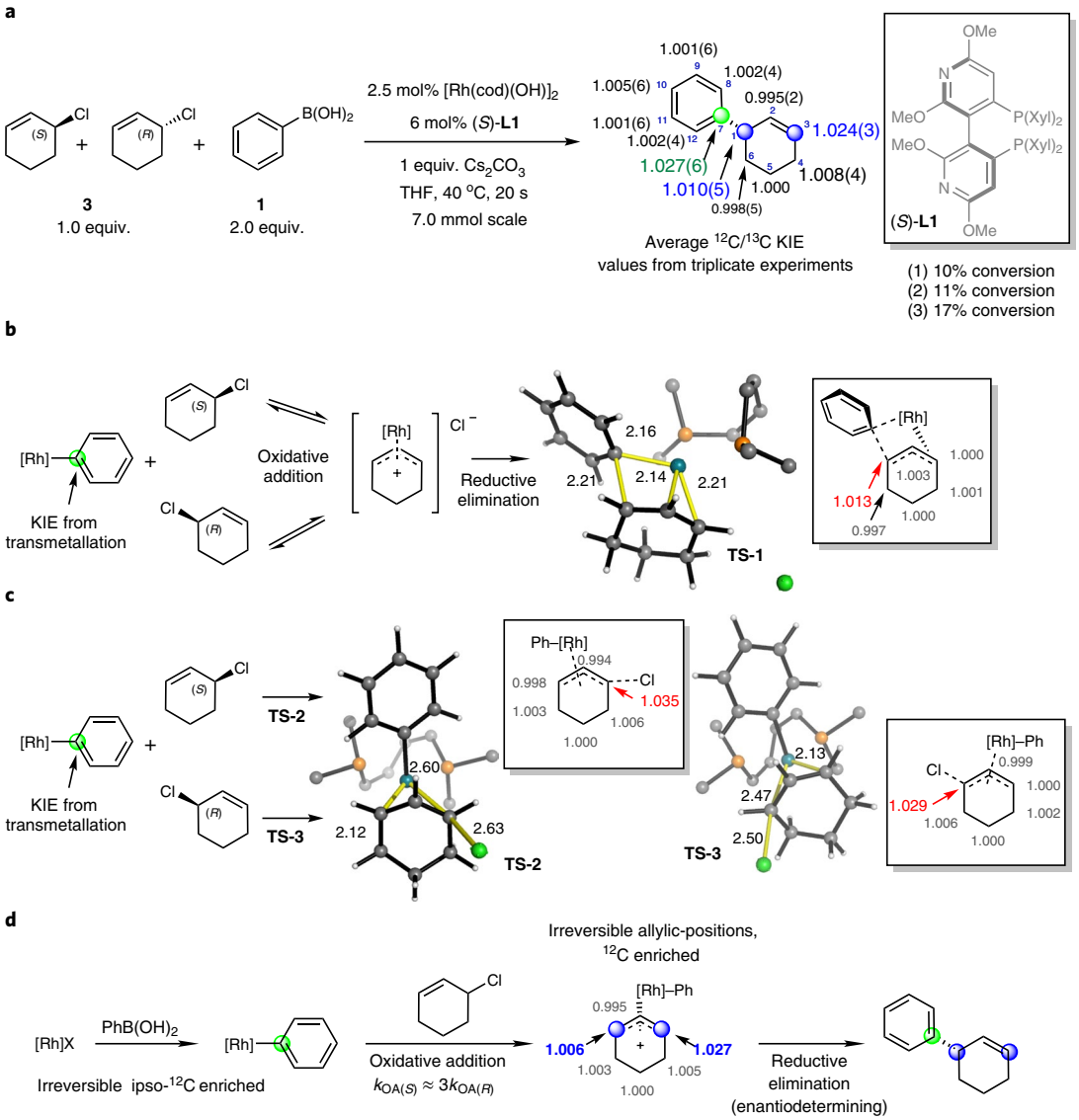

Fig. 3 | Examining the ^{13}C KIE. a, ^{13}C KIE experimental results, standard errors in parenthesis. **b**, Calculated ^{13}C KIEs of a stepwise mechanism with reversible *anti*-oxidative addition followed by irreversible reductive elimination. **c**, Calculated ^{13}C KIEs of a stepwise mechanism with irreversible *anti*-oxidative addition. **d**, Proposed combination of elementary KIEs. A ratio of ~3.3:1 for the oxidative addition of the *S* over the *R* enantiomer of the starting allyl chloride gives the observed level of ^{12}C enrichment. Computed TSs are shown with cropped ligands for clarity; selected distances are shown in Å.

theory with the LANL2TZ(f) ECP/valence triple-ζ basis set for Rh. The Gibbs energy profiles for transmetallation, oxidative addition and reductive elimination steps are illustrated in Fig. 4. Other possible mechanisms were also calculated, but found to have higher reaction barriers (Supplementary Fig. 5).

The calculations suggest that the key process that enable the use of racemic **3** in this DYKAT is oxidative addition to give a common η-**3** intermediate (**V**), in which the stereochemical information of **3** is lost. The energy barrier of oxidative addition for (*R*)-**3** is calculated to be higher than that for (*S*)-**3**, in qualitative agreement with natural abundance ^{13}C KIE experiments. Subsequently, the intermediate undergoes reductive elimination wherein the stereochemistry of the product is set due the spatial constraints the C_2-symmetric ligand imposes on the allyl unit and the phenyl group. From these calculations, we deduced that reductive elimination is enantiodetermining, as the new stereogenic centre is predicted to form irreversibly in this step[50]. The large calculated difference in energy between the reductive elimination TSs ($\Delta\Delta E^{\ddagger}$ = 5.5 kcal mol^{-1} and $\Delta\Delta G^{\ddagger}$ = 7.2 kcal mol^{-1}) is consistent with both the sense and very high levels of enantioselectivity observed experimentally for the formation of (*S*)-**4** in >99% e.e. Transmetallation and oxidative addition steps are both predicted to take place irreversibly. The consequence of an irreversible oxidative addition is that the diastereoselectivity is determined in this step.

Reaction kinetics. The kinetics of the Rh-catalysed reaction of (4-fluoro-3-methylphenyl)boronic acid (**1a**) with cyclohexenyl chloride **3** using ligand (*S*)-**L1** were explored under a range of conditions that ensured that solution-phase reactions, not mass-transfer processes, were rate limiting. Although considerable variation in the rates was found between reactions conducted with various commercial sources of (*S*)-**L1** and $[Rh(cod)(OH)]_2$, kinetic data were found to be reproducible within batches, and all the runs were conducted in triplicate. Temporal concentrations were determined by ^{19}F NMR analysis of a series of eight samples taken at 90 second intervals from the reaction mixtures, over a period of 720 seconds, using 4,4′-difluoro-1,1′-biphenyl as an internal standard for integration.

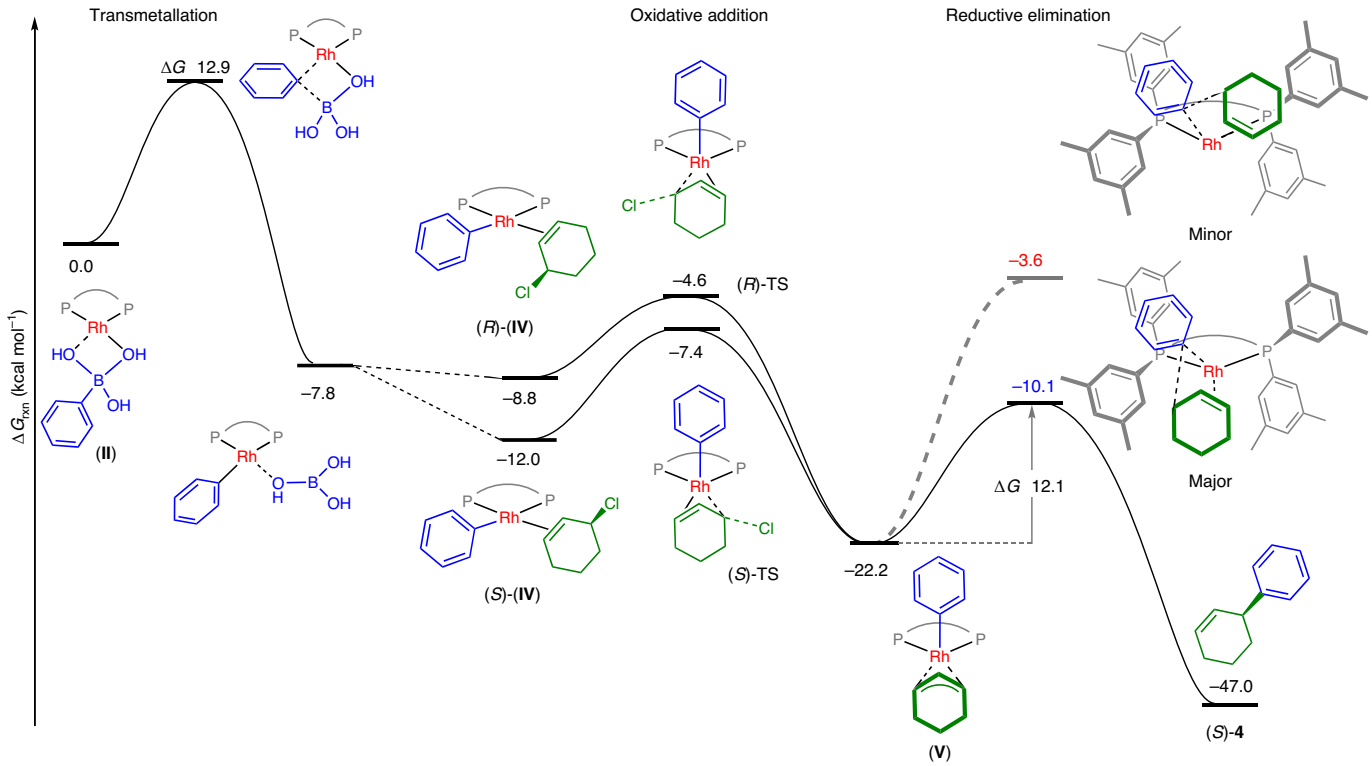

Fig. 4 | A condensed Gibbs energy profile showing transmetallation, oxidative addition and reductive elimination. Geometry optimizations performed at the ωB97X-D/6-31G(d) level of theory with the LANL2DZ(f) ECP basis set for Rh. Single-point energy corrections with an implicit description of the reaction medium by SMD solvent model obtained at the ωB97X-D/6-311+G(d,p) level of theory with the LANL2TZ(f) ECP basis set for Rh.

Systematic variation of the initial concentrations of the cyclohexenyl chloride **3** (0.1, 0.05 and 0.025 M), total Rh (0.0025, 0.005 and 0.0075 M) and the (4-fluoro-3-methylphenyl)boronic acid **1a** (0.1, 0.3 and 0.4 M), afforded product evolution profiles that suggested progressive inhibition:

$$\frac{d[\mathbf{4a}]}{dt} \approx \frac{[Rh]_{TOT}}{a + \frac{b}{[\mathbf{3}]} + \frac{c\,[\mathbf{2}]}{[\mathbf{1a}]}}$$

$a = 9.0 \pm 2.6$ s
$b = 2.3 \pm 0.5 \times 10^{-1}$ M s
$c = 4.2 \pm 0.3 \times 10^{2}$ s

Experiments with exogenous boric acid (**2**) identified inhibition that arose from the accumulating $Cs[B(OH)_4]$ co-product, which is assumed to compete with the arylboronate for coordination to the Rh–OH complex (**I**). All eight datasets could be satisfactorily simulated using a kinetic model based on all of the key mechanistic features evaluated in a pseudo steady-state rate equation (equation (1)) with five concentration terms, $[Rh]_{TOT}$, **4a** (arylation product), **2** (boric acid), **1a** (boronic acid) and **3** (cyclohexenyl chloride), and three simplified empirical constants, *a*, *b* and *c* (Supplementary Figs. 2 and 3). The analysis indicates that the reactions proceed with a first-order dependence on $[Rh]_{TOT}$, and apparent orders in cyclohexenyl chloride **3** and arylboronate **1a** that evolve between limits of pseudo zero order to first order as the reactions proceed, with no simple relationships dominant for either component.

Arylation with heterocyclic and other allyl chlorides. We also calculated the energy profile for the pyranyl substrate **5** and found that the barrier to oxidative addition was much lower than that of **3** (Supplementary Fig. 6). A competition experiment between allyl chlorides **3** and **5** was performed (Fig. 5a). After one hour, the product ratio was 20:1 in favour of product **6**, which indicates that oxidative addition is faster for **5**, which is qualitatively in agreement with the results of our DFT calculations.

Both the ^{13}C KIE experiments and DFT calculations suggest that there are differences in the rate of oxidative addition of the enantiomers of (±)-**3**. Based on this hypothesis, an increase in e.e. of **3** over the course of the reaction would be anticipated. Despite several attempts, the e.e. of **3** could not be reliably measured and enantiopure **3** probably cannot be obtained due to its high reactivity[20], which precludes us from directly probing the relative rate of oxidative addition of the enantiomers of **3**. However, this could be probed using piperidinyl allyl chloride **7**. which was found to be configurationally stable[51].

We monitored the e.e. of **7** under the conditions used in the ^{13}C KIE measurements and found that it increased from 0 to 94% over one hour (Fig. 5b), which supports the idea that the rate of oxidative addition differs for the two enantiomers of the substrate. This also supports our earlier conclusion that a fast interconversion of substrate enantiomers is not required for this asymmetric reaction.

Interestingly, under alternative conditions, previously optimized for **7**, using (*S*)-**L2**, the enantioenrichment of **7** was not observed (Fig. 5d). This observation was unchanged at 30 °C, and so the resolution of starting materials is probably a ligand effect. These ligands impose different steric environments on the oxidative addition TSs, which therefore leads to different relative energies between the oxidative addition TSs of the two enantiomers of the allyl chloride. Under the conditions shown in Fig. 5d, both enantiomers of **7** may react at comparable rates due to the reduced steric constraints in the oxidative addition TSs.

In both of these experiments, we observed that the e.e. of **8** was constant as a function of time, which supports the idea that reductive elimination is the stereodetermining step.

We were able to access enantioenriched (*R*)-**7**[51], and subjected (*R*)-**7** (94% e.e.) to reaction conditions with each enantiomer of **L2** (Fig. 5c). With (*S*)-**L2**, we obtained (*S*)-**8** (95% e.e.), whereas with (*R*)-**L2**, the other enantiomer of the product ((*R*)-**8**, –95% e.e.) was

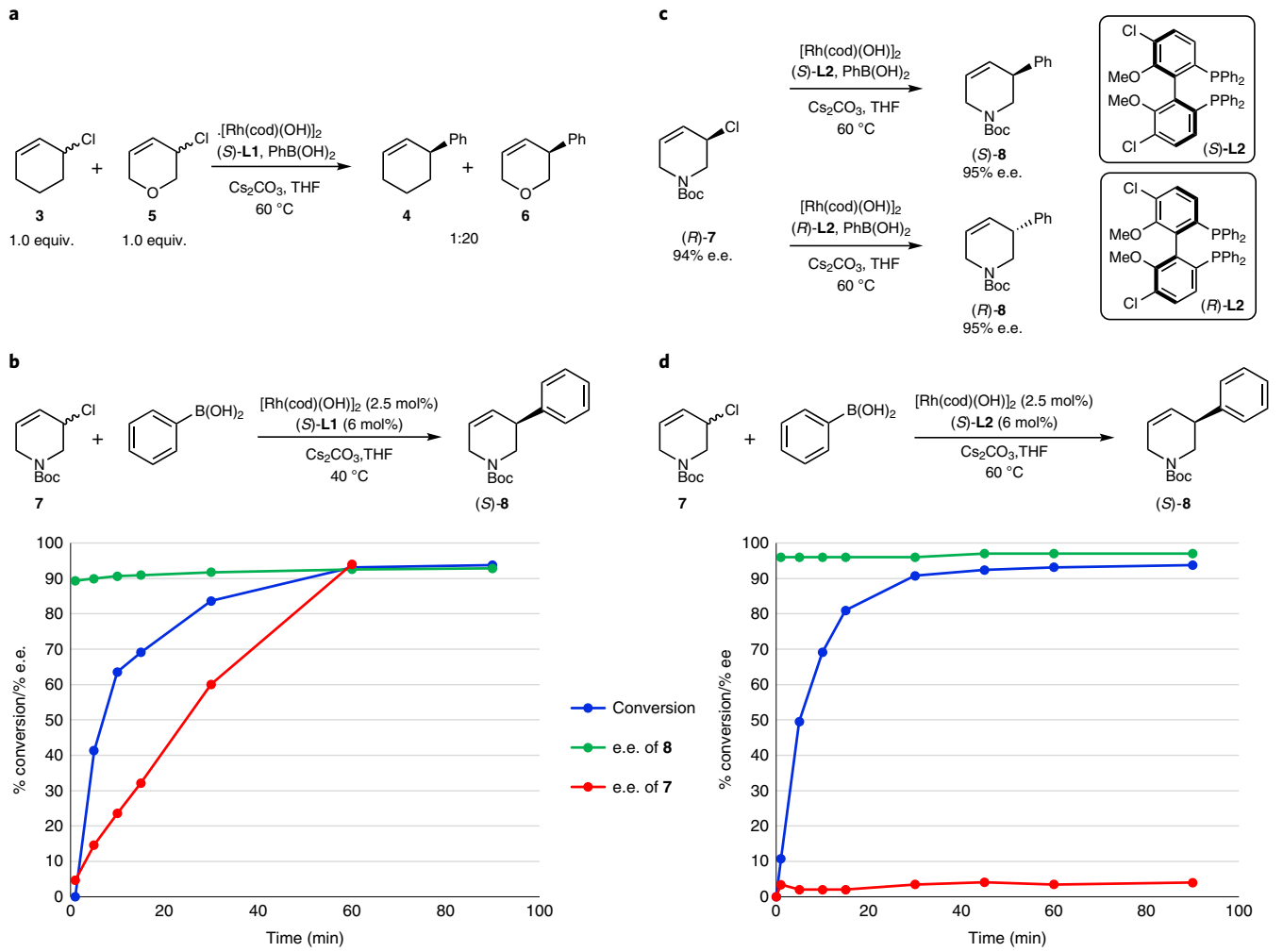

Fig. 5 | Asymmetric allylic arylation with heterocyclic allyl chlorides. a, Competition experiment with allyl chlorides (±)-**3** and (±)-**5** (2.5 mol% [Rh(cod)(OH)]$_2$, 6 mol% **L1**, 1 equiv. PhB(OH)$_2$). A complete conversion of PhB(OH)$_2$ to the arylated product was observed. **b**, The e.e. measured over the course of the reaction with allyl chloride **7** using **L1**. **c**, Arylation of enantioenriched (+)-**7** with both enantiomers of **L2** (2.5 mol% [Rh(cod)(OH)]$_2$, 6 mol% **L2**, 2 equiv. PhB(OH)$_2$), >85% conversion of **7** to the arylated product observed. **d**, The e.e. measured over the course of the reaction with allyl chloride **7** using **L2**.

obtained. Therefore, the absolute stereochemistry of the product is determined by the stereochemistry of the ligand and is not affected by the stereochemistry of the allyl chloride. Interestingly, with (*R*)-**L2**, the reaction was considerably slower, and we observed a deterioration of the e.e. of (*R*)-**7** (from 94 to 82% e.e. over six hours), which suggests that racemization may occur slowly but is not essential for product formation.

Isotopically labelled **7**-*d* was synthesized with a deuterium atom at the vinylic position[51]. Under the conditions shown in Fig. 6a, the addition to (±)-**7**-C3-*d* gave a 1:1 ratio of products with deuterium at C3 and C5. Owing to the ^{2}H label at the vinylic position in each enantiomer of starting material, the two enantiomers could no longer form a common intermediate after oxidative addition. One enantiomer reacts to give one intermediate which, after reductive elimination, leads to one pseudo-regioisomer of the product, and the other reacts to give the alternative pseudo-regioisomer.

Therefore, if enantioenriched ^{2}H-labelled **7** is used the products should have an excess of the deuterium label at one position (allylic or vinylic) depending on the stereochemistry of the ligand used. After subjecting (*R*)-**7**-C3-*d* (94% e.e.) to optimized reaction conditions with (*S*)-**L2**, the majority of deuterium remained at C3 in product (*S*)-**8**, whereas with (*R*)-**L2**, the majority of deuterium was found at the allylic position of (*R*)-**7** (Fig. 6b).

Deuterium-labelled substrates can be used to assess the stereochemical outcome of the individual steps of allylic substitution reactions[52–55]. According to our proposed mechanism of *anti*-oxidative addition, we expected ((*R*)-**7**-C3-*d*) to give the opposite results obtained in terms of the observed pseudo-regioisomer preference with each enantiomer of the ligand. Our experimental results surprisingly indicate that with **7**, *syn*-oxidative addition is the major pathway. In each case, there is a small percentage of deuterium scrambling (7:1 ratio), which we attribute to a 7:1 ratio of the *syn*- and *anti*-oxidative addition steps that occur. At this stage, we cannot rule out that the scrambling is due to slow racemization of **7** over the course of the reaction, or alternatively to isomerization after oxidative addition via nucleophilic displacement with Rh(I) species, in analogy to mechanistic pathways observed in Pd(0) catalysis[56].

Recently, we discovered that the related Rh-catalysed enantioselective additions to fused bicyclic substrates give stereochemical results consistent with *syn*-selective addition to racemic allyl chloride starting materials (Fig. 6c)[14]. To further probe these experimental results, we compared the *syn*- and *anti*-TSs that arise from oxidative addition to **9** using DFT calculations (see Fig. 7a for the favoured *syn*-TS). The results show that steric clash between the substrates acetal bridge and ligand used is key to determining the facial selectivity of oxidative addition. It is important to note here

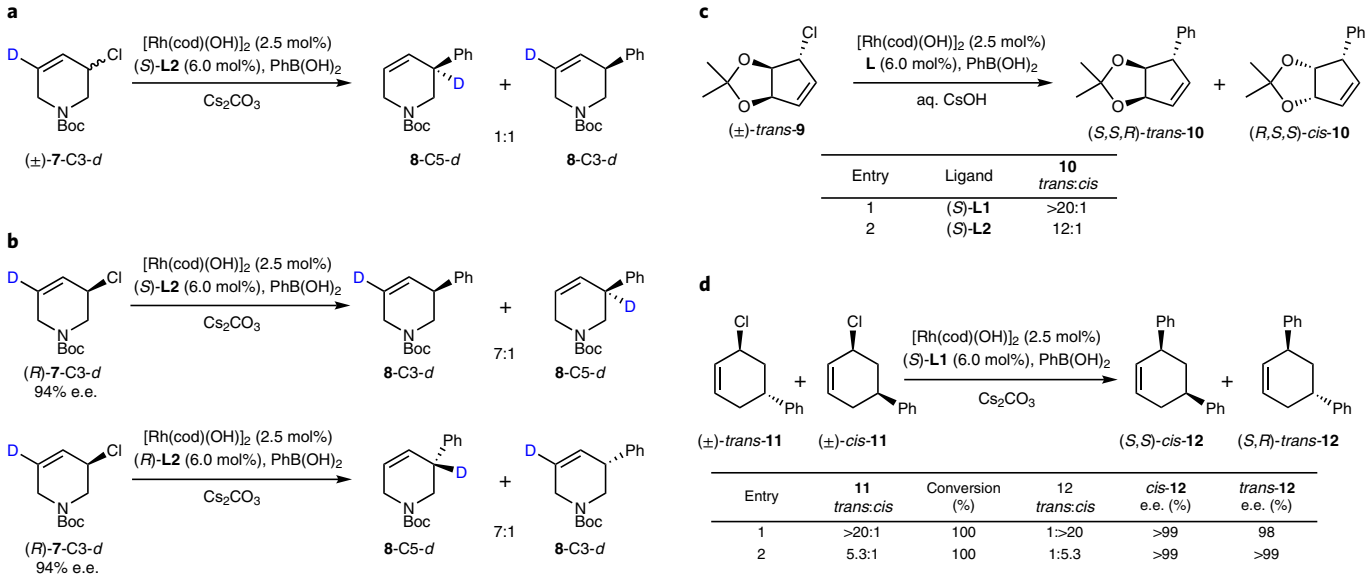

Fig. 6 | Asymmetric allylic arylation with deuterium-labelled allyl chlorides and diastereomeric allyl chlorides. a, Arylation of (±)-*d*-**7**. **b**, Arylation of (*R*)-*d*-**7** with both enantiomers of **L2**. **c**, Arylation of bicyclic substrate **9** showing evidence for *syn*-oxidative addition. **d**, Arylation of diastereomeric 5-phenyl-substituted starting materials showing evidence for *anti*-oxidative addition. All the reactions were performed in THF at 60 °C.

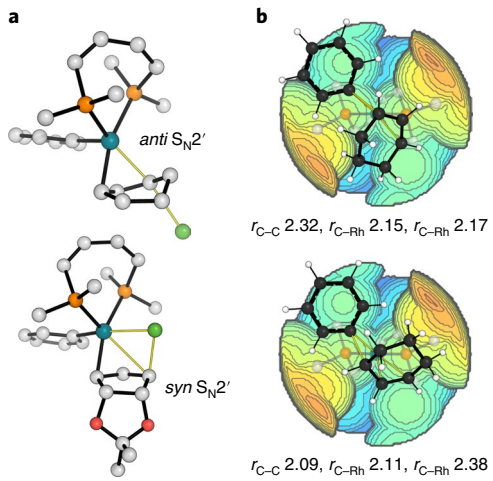

Fig. 7 | Simplified models showing the origins of diastereoselectivity and enantioselectivity in this Rh(I)-catalysed asymmetric Suzuki–Miyaura coupling. (**a**) Favoured *anti*-oxidative addition TS for **3** and favoured *syn*-oxidative addition TS for **9**. (**b**) Reductive elimination TSs for **3**. Catalytic pocket images generated using: SambVca 2.1[52].

that oxidative addition is the diastereodetermining step in this system, whereas reductive elimination remains in control of the absolute stereochemistry.

DFT calculations for model substrate **3** (Figs. 4 and 7) clearly indicate that in **3** *anti*-oxidative addition is favoured. We have also examined enantioselective additions to phenyl-substituted allyl chlorides[11], where mixtures of the four stereoisomers of 3-chloro-5-phenylcyclohex-1-ene (**11**) gave overall enantioselective inversion to *cis*- and *trans*-**12** (Fig. 6d). These experiments, where we observe highly enantioselective overall inversion to form *cis*- and *trans*-**12**, are consistent with *anti*-oxidative addition with an aryl-Rh species, followed by inner-sphere attack of the aryl nucleophile, delivering the phenyl on the same side of the allyl ion as the Rh.

Therefore, we have experimentally observed and computationally validated that Rh species can add to allyl halide substrates *via syn*- or *anti*-oxidative addition, depending on the steric accessibility of the substrate (Fig. 7a). The oxidative addition step dictates diastereoselectivity and is influenced by the substrate, whereas the overall sense of enantioselectivity is catalyst-controlled and set in the reductive elimination step. The high enantioselectivity observed experimentally is reflected in the large difference in energy between the reductive elimination TSs. This can be attributed to steric effects between the ligand and allyl fragment, which in turn give rise to substantial differences in key bond distances between the two competing TSs. An analysis of the catalytic pocket (Fig. 7b) emphasizes the narrow groove provided by the ligand in which the reductive elimination must take place[57]. The minor TS structure has a weaker coordination between the alkene and Rh, and a much shorter forming C–C bond (that is, a later TS), compared with the favoured structure, which is consistent with the large energy difference between the two.

Conclusions

The asymmetric Suzuki–Miyaura coupling of arylboronic acids with racemic allylic halides catalysed by a Rh(I) complex gives highly enantioenriched arylated products. We have used a variety of techniques to elucidate a mechanistic proposal and the key mechanistic features of this proposal are fully consistent with a detailed analysis of the reaction kinetics. Here the active catalytic species is monomeric in Rh and ligand, and irreversible transmetallation between boron and Rh is the first step in the catalytic cycle. Experimentally observed natural abundance ^{13}C KIEs in combination with theoretical calculations are key to demonstrating that oxidative addition occurs in a ~3.3:1 ratio in favour of one enantiomer over the other. A common pseudo-symmetrical η^3 Rh–allyl complex is formed by the irreversible oxidative addition of Rh–aryl intermediates to both enantiomers of the racemic substrates. Interestingly, oxidative addition can occur in a *syn* or *anti* fashion depending on the steric accessibility of the substrate. The symmetry of η^3 Rh–allyl complexes formed by oxidative addition was probed using configurationally stable, racemic, enantiomerically enriched and deuterium labelled piperidinyl allyl chlorides along with racemic diastereomeric

substituted allyl chlorides. These studies support the proposed promiscuity of the oxidative addition step and demonstrate that the reductive elimination of common intermediates formed from both enantiomers give highly enantioenriched products, in which the diastereoselectivity is determined by oxidative addition and the absolute stereochemistry of the product is dictated by the ligand.

We foresee that this study will contribute to the broader understanding of asymmetric Rh–allyl chemistry and will enable the discovery, exploitation and understanding of new asymmetric reactions with racemic substrates.

Methods

Instrumentation and materials. Procedures using oxygen and/or moisture-sensitive materials were performed with anhydrous solvents under an atmosphere of argon in flame-dried flasks, using standard Schlenk techniques. Dry THF and CH_2Cl_2 were collected fresh from an mBraun SPS-800 solvent purification system having been passed through anhydrous alumina columns. THF-d_8 was purchased from Fluorochem and degassed using freeze–thaw cycles and kept under argon over 3 Å molecular sieves. Other deuterated solvents were purchased from Sigma-Aldrich. Unless stated otherwise, commercially available reagents were purchased from Sigma-Aldrich, Fisher Scientific, Apollo Scientific, Acros Organics, Strem Chemicals, Alfa Aesar or TCI UK and were used without purification. $[Rh(cod)(OH)]_2$ was purchased from Sigma Aldrich.

Analytical thin-layer chromatography was performed on precoated glass-backed plates (Silica Gel 60 F254; Merck) and visualized using a combination of ultraviolet light (254 nm) and aqueous ceric ammonium molybdate, aqueous basic potassium permanganate stains or *p*-anisaldehyde solution. Flash column chromatography was carried out using Apollo Scientific silica gel 60 (0.040–0.063 nm), Merck 60 Å silica gel, VWR (40–63 µm) silica gel and Sigma Aldrich silica gel. Pressure was applied at the column head *via* a flow of nitrogen. Heating was performed using DrySyn heating blocks and the heating plate of the stirrer or using a Julabo FT902 immersion cooler.

Unless stated otherwise, solution NMR spectra were recorded at room temperature; ^{1}H, ^{2}H, ^{13}C, ^{31}P, ^{11}B, ^{19}F NMR and two-dimensional NMR experiments were carried out using a Bruker AVIII HD 400 (400/100 MHz), AVIII HD 500 (500/125 MHz) or AVII 500 (500/125 MHz) spectrometer. Chemical shifts (δ) are reported in ppm from the residual solvent peak and coupling constants (J) are quoted in Hz. Assignments were made with the assistance of gradient correlation spectroscopy, gradient heteronuclear single quantum coherence, gradient heteronuclear multiple bond coherence or nuclear Overhauser effect NMR spectra.

Chiral HPLC separations were achieved using an Agilent 1230 Infinity series normal-phase HPLC unit and HP Chemstation software. Chiralpak columns (250 × 4.6 mm), fitted with matching Chiralpak Guard Cartridges (10 × 4 mm), were used as specified in the text. Solvents used were of HPLC grade (Fisher Scientific, Sigma Aldrich or Rathburn); all the eluent systems were isocratic. Chiral SFC separations were conducted on a Waters Acquity UPC2 (ultraperformance convergence chromatography) system equipped with a fluid delivery module (a liquid CO_2 pump and a modifier pump), a sampler manager (FL autosampler), a heated column manager 30S fitting eight installed columns and a photodiode array detector. Daicel Chiralpak IA-3, IB-3, IC-3, ID-3, IE-3, IF-3 or IG-3 columns were used as indicated.

Low-resolution and high-resolution mass spectral analyses were acquired by electrospray ionization, electron impact and/or field ionization. Low-resolution electrospray ionization was recorded using an Agilent 6120 Quadrupole LC/MS. High-resolution accurate electrospray ionization was recorded using a Thermo Exactive 1.1 SP5 Benchtop orbitrap mass spectrometer and electron impact and/or field ionization on a Waters GTC temperature-programmed solid probe inlet within the Department of Chemistry, University of Oxford. Infrared measurements were carried out using a Bruker Tensor 27 FT-IR with internal calibration in the range 600–4,000 cm^{-1}. Optical rotations were recorded on a Schmidt Haensch Unipol L2000 Polarimeter at 20 °C in a 10 cm cell in the stated solvent; $[\alpha]_D$ values are given in 10^{-1} deg cm^2 g^{-1} (concentration c given as g per 100 ml).

Computational methods. All the DFT calculations were performed with the Gaussian 09 program[48] using the ωB97X-D functional. The split-valence 6-31G(d) basis set was used for the C, N, O, H, P and Cl atoms, and the LANL2DZ(f)3 (orbital exponent of 1.35) ECP/valence double zeta basis set with an *f* polarization function for Rh was used in all the geometry optimizations. Single-point energy corrections were obtained at the ωB97X-D /6-311+G(d,p) level of theory for the C, N, O, H, P and Cl atoms, and the ωB97X-D/LANL2TZ(f)4 ECP/valence triple zeta basis set with an *f* polarization function for Rh with an implicit description of the reaction medium (THF) by the SMD solvent model was implemented in Gaussian09.

Gibbs free energies were evaluated at 333 K (the reaction temperature), for which the vibrational entropy contributions were computed using a free-rotor approximation for low-frequency modes. A cutoff frequency of 100 cm^{-1} was used as we switched between the rigid-rotor harmonic oscillator approximation for vibrations above this value and the free-rotor approximation below it. For all the mechanistic studies, a conventional standard state of 1 $mol l^{-1}$ in solution for all the species was employed. Harmonic vibrational frequencies were computed for all the stationary points to confirm them as either minima or TSs, which possesses zero or a single imaginary frequency, respectively. All energetic terms are reported in kcal mol^{-1}. Molecular structures were visualized within the PyMOL Molecular Graphics System, Version 1.8 Schrödinger, LLC.

Data availability

Detailed experimental methods and analytical data for all the experiments, along with absolute energies and selected distances for the DFT-computed structures and for the computed stationary points, can be found in the Supplementary Information. Cartesian coordinates (in *xyz* format) for the computed stationary points can be found in the Supplementary Data.

Code availability

All Python scripts used for the data analysis have been made available at https://github.com/bobbypaton under a creative commons CC-BY license.

Received: 15 July 2019; Accepted: 15 February 2021;
Published online: 5 April 2021

References

1. Hall, D. G. *Boronic Acids: Preparation and Applications in Organic Synthesis and Medicine* (Wiley-VCH, 2006).
2. Suzuki, A. Cross-coupling reactions of organoboranes: an easy way to construct C–C bonds (Nobel Lecture). *Angew. Chem. Int. Ed.* **50**, 6722–6737 (2011).
3. Cherney, A. H., Kadunce, N. T. & Reisman, S. E. Enantioselective and enantiospecific transition-metal-catalyzed cross-coupling reactions of organometallic reagents to construct C–C bonds. *Chem. Rev.* **115**, 9587–9652 (2015).
4. Dong, L. et al. Asymmetric nitroallylation of arylboronic acids with nitroallyl acetates catalyzed by chiral rhodium complexes and its application in a concise total synthesis of optically pure (+)-γ-lycorane. *Org. Lett.* **7**, 4285–4288 (2005).
5. Yu, B., Menard, F., Isosno, N. & Lautens, S. Synthesis of homoallylic alcohols via Lewis acid assisted enantioselective desymmetrization. *Synthesis* **2009**, 853–859 (2009).
6. Shintani, R., Takatsu, K., Takeda, M. & Hayashi, T. Copper-catalyzed asymmetric allylic substitution of allyl phosphates with aryl- and alkenylboronates. *Angew. Chem. Int. Ed.* **50**, 8656–8659 (2011).
7. Zhang, P., Brozek, L. A. & Morken, J. P. Pd-catalyzed enantioselective allyl–allyl cross-coupling. *J. Am. Chem. Soc.* **132**, 10686–10688 (2010).
8. Chung, K., Miyake, Y. & Uemura, S. Nickel(0)-catalyzed asymmetric cross-coupling reactions of allylic compounds with Grignard reagents using optically active oxazolinylferrocenylphosphines as ligands. *J. Chem. Soc. Perkin Trans. 1* **2000**, 2725–2729 (2000).
9. Ohmiya, H., Makida, Y., Tanaka, T. & Sawamura, M. Palladium-catalyzed γ-selective and stereospecific allyl—aryl coupling between allylic acetates and arylboronic acids. *J. Am. Chem. Soc.* **130**, 17276–17277 (2008).
10. Ohmiya, H., Yokokawa, N. & Sawamura, M. Copper-catalyzed gamma-selective and stereospecific allyl–aryl coupling between (*Z*)-acyclic and cyclic allylic phosphates and arylboronates. *Org. Lett.* **12**, 2438–2440 (2010).
11. Sidera, M. & Fletcher, S. P. Rhodium-catalyzed asymmetric allylic arylation of racemic halides with arylboronic acids. *Nat. Chem.* **7**, 935–939 (2015).
12. Schäfer, P., Palacin, T., Sidera, M. & Fletcher, S. P. Asymmetric Suzuki–Miyaura coupling of heterocycles via rhodium-catalyzed allylic arylation of racemates. *Nat. Commun.* **8**, 15762 (2017).
13. González, J., van Dijk, L., Goetzke, F. W. & Fletcher, S. P. Highly enantioselective rhodium-catalyzed cross-coupling of boronic acids and racemic allyl halides. *Nat. Protocols* **14**, 2972–2985 (2019).
14. Goetzke, F. W., Mortimore, M. & Fletcher, S. P. Enantio- and diastereoselective Suzuki–Miyaura coupling with racemic bicycles. *Angew. Chem. Int. Ed.* **58**, 12128–12132 (2019).
15. Hayashi, T., Takahashi, M., Takaya, Y. & Ogasawara, M. Catalytic cycle of rhodium-catalyzed asymmetric 1,4-addition of organoboronic acids. Arylrhodium, oxa-π-allylrhodium, and hydroxorhodium intermediates. *J. Am. Chem. Soc.* **124**, 5052–5058 (2002).
16. Kina, A., Iwamura, H. & Hayashi, T. A kinetic study on Rh/binap-catalyzed 1,4-addition of phenylboronic acid to enones: negative nonlinear effect caused by predominant homochiral dimer contribution. *J. Am. Chem. Soc.* **128**, 3904–3905 (2006).
17. Jacobsen, E. N., Pfaltz, A. & Yamamoto, H. *Comprehensive Asymmetric Catalysis II* (Springer, 1999).

18. Turnbull, B. W. H. & Evans, P. A. Asymmetric rhodium-catalyzed allylic substitution reactions: discovery, development and applications to target-directed synthesis. *J. Org. Chem.* **83**, 11463–11479 (2018).
19. You, H., Rideau, E., Sidera, M. & Fletcher, S. P. Non-stabilized nucleophiles in Cu-catalyzed dynamic kinetic asymmetric allylic alkylation. *Nature* **517**, 351–355 (2015).
20. Rideau, E., You, H., Sidera, M., Claridge, T. D. W. & Fletcher, S. P. Mechanistic studies on a Cu-catalyzed asymmetric allylic alkylation with cyclic racemic starting materials. *J. Am. Chem. Soc.* **139**, 5614–5624 (2017).
21. Lu, Z., Wilsily, A. & Fu, G. C. Stereoconvergent amine-directed alkyl–alkyl Suzuki reactions of unactivated secondary alkyl chlorides. *J. Am. Chem. Soc.* **133**, 8154–8157 (2011).
22. Gutierrez, O., Tellis, J. C., Primer, D. N., Molander, G. A. & Kozlowski, M. C. Nickel-catalyzed cross-coupling of photoredox-generated radicals: uncovering a general manifold for stereoconvergence in nickel-catalyzed cross-couplings. *J. Am. Chem. Soc.* **137**, 4896–4899 (2015).
23. Langlois, J., Emery, D., Mareda, J. & Alexakis, A. Mechanistic identification and improvement of a direct enantioconvergent transformation in copper-catalyzed asymmetric allylic alkylation. *Chem. Sci.* **3**, 1062–1069 (2012).
24. Girard, C. & Kagan, H. B. Nonlinear effects in asymmetric synthesis and stereoselective reactions: ten years of investigation. *Angew. Chem. Int. Ed.* **37**, 2922–2959 (1998).
25. Tsui, G. C., Menard, F. & Lautens, M. Regioselective rhodium(I)-catalyzed hydroarylation of protected allylic amines with arylboronic acids. *Org. Lett.* **12**, 2456–2459 (2010).
26. Yang, Q., Wang, Y., Luo, S. & Wang, J. Kinetic resolution and dynamic kinetic resolution of chromene by rhodium-catalyzed asymmetric hydroarylation. *Angew. Chem. Int. Ed.* **58**, 5343–5347 (2019).
27. Yang, X. et al. Catalytic hydrothiolation: counterion-controlled regioselectivity. *J. Am. Chem. Soc.* **141**, 3006–3013 (2019).
28. Mc Daniel, D. H. & Brown, H. C. An extended table of Hammett substituent constants based on the ionization of substituted benzoic acids. *J. Org. Chem.* **23**, 420–427 (1958).
29. Corrie, T. J. A., Ball, L. T., Russell, C. A. & Lloyd-Jones, G. C. Au-catalyzed biaryl coupling to generate 5- to 9-membered rings: turnover-limiting reductive elimination versus π-complexation. *J. Am. Chem. Soc.* **139**, 245–254 (2017).
30. Lennox, A. J. J. & Lloyd-Jones, G. C. Transmetalation in the Suzuki–Miyaura coupling: the fork in the trail. *Angew. Chem. Int. Ed.* **52**, 7362–7370 (2013).
31. Thomas, A. A. & Denmark, S. E. Pre-transmetalation intermediates in the Suzuki–Miyaura reaction revealed: the missing link. *Science* **352**, 329–332 (2016).
32. Yaman, T. & Harvey, J. N. Suzuki–Miyaura coupling revisited: an integrated computational study. *Faraday Discuss.* **220**, 425–442 (2019).
33. Singleton, D. A. & Thomas, A. A. High-precision simultaneous determination of multiple small kinetic isotope effects at natural abundance. *J. Am. Chem. Soc.* **117**, 9357–9358 (1995).
34. Frantz, D. E., Singleton, D. A. & Snyder, J. P. ^{13}C kinetic isotope effects for the addition of lithium dibutylcuprate to cyclohexenone. Reductive elimination is rate-determining. *J. Am. Chem. Soc.* **119**, 3383–3384 (1997).
35. Li, J. et al. Catalytic asymmetric cascade vinylogous Mukaiyama 1,6-Michael/Michael addition of 2-silyloxyfurans with azoalkenes: direct approach to fused butyrolactones. *J. Am. Chem. Soc.* **137**, 10124–10127 (2015).
36. Colletto, C., Islam, S., Juliá-Hernández, F. & Larrosa, I. Room-temperature direct β-arylation of thiophenes and benzo[b]thiophenes and kinetic evidence for a Heck-type pathway. *J. Am. Chem. Soc.* **138**, 1677–1683 (2016).
37. Smith, J. R. et al. Enantioselective rhodium(III)-catalyzed Markovnikov hydroboration of unactivated terminal alkenes. *J. Am. Chem. Soc.* **139**, 9148–9151 (2017).
38. Rathbun, C. M. & Johnson, J. B. Rhodium-catalyzed acylation with quinolinyl ketones: carbon–carbon single bond activation as the turnover-limiting step of catalysis. *J. Am. Chem. Soc.* **133**, 2031–2033 (2011).
39. Moore, J. L., Silvestri, A. P., de Alaniz, J. R., DiRocco, D. A. & Rovis, T. Mechanistic investigation of the enantioselective intramolecular Stetter reaction: proton transfer is the first irreversible step. *Org. Lett.* **13**, 1742–1745 (2011).
40. Lee, D. H., Kwon, K. H. & Yi, C. S. Selective catalytic C–H alkylation of alkenes with alcohols. *Science* **333**, 1613–1616 (2011).
41. Meyer, M. P. *New Applications of Isotope Effects in the Determination of Organic Reaction Mechanisms* (Elsevier, 2012).
42. Vo, L. K. & Singleton, D. A. Isotope effects and the nature of stereo- and regioselectivity in hydroaminations of vinylarenes catalyzed by palladium(II)–diphosphine complexes. *Org. Lett.* **6**, 2469–2472 (2004).
43. Roytman, V. A., Karugu, R. W., Hong, Y., Hirschi, J. S. & Vetticatt, M. J. ^{13}C kinetic isotope effects as a quantitative probe to distinguish between enol and enamine mechanisms in aminocatalysis. *Chem. Eur. J.* **24**, 8098–8102 (2018).
44. Wolfsberg, M., Van Hook, W. A., Paneth, P. & Rebelo, L. P. N. *Isotope Effects in the Chemical, Geological, and Bio Sciences* (Springer, 2010).
45. Simmons, E. M. & Hartwig, J. F. On the interpretation of deuterium kinetic isotope effects in C–H bond functionalizations by transition-metal complexes. *Angew. Chem. Int. Ed.* **51**, 3066–3072 (2012).
46. Deb, A., Hazra, A., Peng, Q., Paton, R. S. & Maiti, D. Detailed mechanistic studies on palladium-catalyzed selective C–H olefination with aliphatic alkenes—a significant influence of proton shuttling. *J. Am. Chem. Soc.* **139**, 763–775 (2017).
47. Mekareeya, A. et al. Mechanistic insight into palladium-catalyzed cycloisomerization: a combined experimental and theoretical study. *J. Am. Chem. Soc.* **139**, 10104–10114 (2017).
48. Frisch, M. J. et al. *Gaussian 09, Revision D.01* (Gaussian, 2009).
49. Straker, R., Peng, Q., Mekareeya, A., Paton, R. S. & Anderson, E. A. Computational ligand design in enantio- and diastereoselective ynamide [5+2] cycloisomerizations. *Nat. Commun.* **7**, 10109 (2016).
50. Peng, Q., Duarte, F. & Paton, R. S. Computing organic stereoselectivity—from concepts to quantitative calculations and predictions. *Chem. Soc. Rev.* **45**, 6093–6107 (2016).
51. Karabiyikoglu, S., Brethomé, A., Palacin, T., Paton, R. S. & Fletcher, S. P. Enantiomerically enriched tetrahydropyridine allyl chlorides. *Chem. Sci.* **11**, 4125–4130 (2020).
52. Mackenzie, P. B., Whelan, J. & Bosnich, B. Asymmetric synthesis. Mechanism of asymmetric catalytic allylation. *J. Am. Chem. Soc.* **107**, 2046–2054 (1985).
53. Lloyd-Jones, G. C. & Stephen, S. C. Memory effects in Pd-catalysed allylic alkylation: stereochemical labelling through isotopic desymmetrization. *Chem. Eur. J.* **4**, 2539–2549 (1998).
54. Lloyd-Jones, G. C. et al. Conclusive evidence for a retention–retention pathway for the molybdenum-catalyzed asymmetric alkylation. *J. Am. Chem. Soc.* **126**, 702–703 (2004).
55. Madrahimov, S. T. & Hartwig, J. F. Origins of enantioselectivity during allylic substitution reactions catalyzed by metallacyclic iridium complexes. *J. Am. Chem. Soc.* **134**, 8136–8147 (2012).
56. Granberg, K. L. & Bäckvall, J. E. Isomerization of (π-allyl)palladium complexes via nucleophilic displacement by palladium(0). A common mechanism in palladium(0)-catalyzed allylic substitution. *J. Am. Chem. Soc.* **114**, 6858–6863 (1992).
57. Falivene, L. et al. Towards the online computer-aided design of catalytic pockets. *Nat. Chem.* **11**, 872–879 (2019).

Acknowledgements

The EPSRC supports this work though standard grant EP/N022246/1. L.v.D. and R.A. thank the EPSRC Centre for Doctoral Training (CDT) in Synthesis for Biology and Medicine (EP/L015838/1) for studentships, generously supported by AstraZeneca, Diamond Light Source, Defence Science and Technology Laboratory, Evotec, GlaxoSmithKline, Janssen, Novartis, Pfizer, Syngenta, Takeda, UCB and Vertex. R.A. also acknowledges the Development and Promotion of Science and Technology Talents Project and the Royal Thai Government. This material is based on work supported by the National Science Foundation under Grant no. 1955876. We used the Dirac cluster at Oxford supported by the EPSRC CDT for Theory and Modelling in Chemical Sciences (EP/L015722/1), the RMACC Summit supercomputer, which is supported by the National Science Foundation (ACI-1532235 and ACI-1532236), the University of Colorado Boulder and Colorado State University, and the Extreme Science and Engineering Discovery Environment (XSEDE) through allocation TG-CHE180056 and computing resources provided by the National e-Science Infrastructure Consortium, Thailand. O.S. thanks the Scientific and Technological Research Council of Turkey for the 2214-A Scholarship Programme. The research leading to these results has received funding from the European Research Council under the European Union's Seventh Framework Programme (FP7/2007-2013)/ERC grant agreement no. [838616].

Author contributions

S.P.F. conceived and directed the project. S.P.F., L.v.D. and M.S. designed the experiments. L.v.D., M.S. and S.K. performed the experiments. L.v.D., R.A., M.S., R.S.P., G.C.L.-J. and S.P.F. analysed the experimental results. R.S.P, L.v.D., R.A. and O.S. designed, conducted and analysed the computational work. T.D.W.C. designed and performed the ^{13}C NMR experiments. G.C.L.-J. derived the pseudo steady-state rate equation. L.v.D. and S.P.F. wrote the manuscript with contributions from R.S.P., G.C.L.-J., T.D.W.C., M.S. and R.A.

Competing interests

The authors declare no competing interests.

Additional information

Supplementary information The online version contains supplementary material available at https://doi.org/10.1038/s41929-021-00589-y.

Correspondence and requests for materials should be addressed to T.D.W.C., G.C.L.-J., R.S.P. or S.P.F.

Peer review information *Nature Catalysis* thanks Per-Ola Norrby and the other, anonymous, reviewer(s) for their contribution to the peer review of this work.

Reprints and permissions information is available at www.nature.com/reprints.

Publisher's note Springer Nature remains neutral with regard to jurisdictional claims in published maps and institutional affiliations.